Numerical Framework for the Investigation of a Transpiration Cooled LOx/LH$_2$ Rocket Engine Combustion Chamber

Jonas Peichl★ [†], *Markus Selzer*★,*Tatjana Cziep*★, *Patrick Pfannes* ★,*, *Hannah Böhrk*★,**,
Andreas Schwab★★, *Jens von Wolfersdorf*★★, *Patrick Palmetshofer*★★,★★★ *and Daniel Eiringhaus*★★★
★*Institute of Structures and Design, German Aerospace Center*
Pfaffenwaldring 38-40, 70569 Stuttgart, Germany
★★*Institute of Aerospace Thermodynamics, University of Stuttgart*
Pfaffenwaldring 31, 70569 Stuttgart, Germany
★★★*ArianeGroup GmbH*
Robert-Koch-Straße 1, 82024 Taufkirchen, Germany
jonas.peichl@dlr.de · markus.selzer@dlr.de · tatjana.cziep@dlr.de
Hannah.Boehrk@dhbw-stuttgart.de
andreas.schwab@itlr.uni-stuttgart.de · jens.von-wolfersdorf@itlr.uni-stuttgart.de
patrick.palmetshofer@itlr.uni-stuttgart.de · daniel.eiringhaus@ariane.group
[†]Corresponding author, ∗ now at MTU Aero Engines ∗∗ now at DHBW Stuttgart

Abstract

The aim of this study is to present a numerical framework for the development of transpiration cooled rocket combustion chambers based on the commercial CFD software ANSYS CFX. The framework couples the hot gas flow domain and the coolant reservoir domain with the porous domain. The numerical setup is applied to an exemplary virtual transpiration cooled LOx/LH$_2$ main stage rocket engine. Two different approaches modeling the hot gas flow with non-reactive flow and reactive flow are introduced and evaluated. The described setup was used for a parametric study to identify desirable properties for the porous material.

1. Introduction

The propulsion system of future space transportation systems faces multiple challenges, with rising thermal and mechanical loads on the engine structure on one hand and the demand for enhanced engine life time for reusable rocket engines and a radical cost reduction on the other hand. A special emphasis has to be laid on the thermal design of the thermally highly loaded combustion chamber structure, with wall heat fluxes in the nozzle throat region reaching over 80 MW/m^2 for the European Vulcain rocket engine.[25] In order to protect the combustion chamber structure from such high thermal loads, effective cooling methods have to be applied.

For main stage engines, regenerative cooling is the state-of the-art cooling method. The fuel used as a coolant is forced through backside cooling channels in the combustion chamber wall, reducing the hot gas side wall temperature through conductive heat transfer in the wall and convective heat transfer in the cooling channel. This cooling method is advantageous due to the complete usage of the fuel as propellant in a closed regenerative system, hence reducing performance losses, and furthermore heating the fuel before the injection which is beneficial to combustion stability. However, regenerative cooling for the extreme thermal loads in a combustion chamber requires thin wall structures made of highly conductive materials. This design is prone to thermo-mechanical low cycle fatigue, known as the doghouse effect. Furthermore, the small cooling channels induce high pressure losses which are typically between 5%-25% of the combustion chamber pressure.[26] The hydraulic losses in the cooling channels have to be compensated by the engine turbopump system, leading to a higher system mass.

Future rocket engines, which aim to provide higher performance due to elevated combustion chamber pressures therefore have to cope with even higher thermal loads as well as an elevated engine life time due to the demand for reusability. Therefore novel cooling approaches are being considered. An innovative approach for cooling rocket engine combustion chambers is transpiration cooling. Figure 1 schematically illustrates the processes at a transpiration cooled wall. The wall consists of a porous material which is perfused by a coolant fluid. When the fluid passes through the
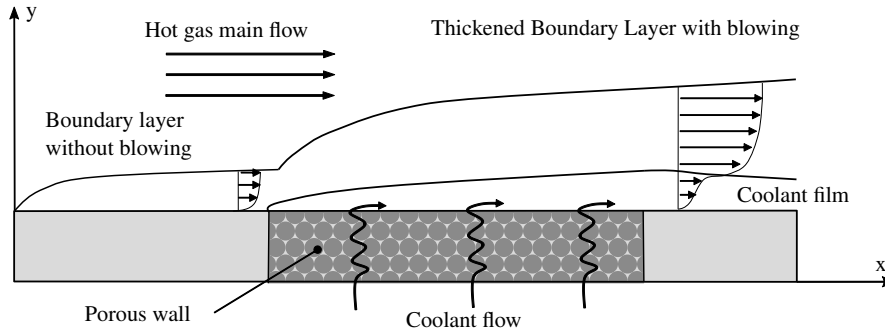
Figure 1: Schematic description of transpiration cooling[23]

porous wall, it cools the solid structure by internal convective cooling. Additionally, the coolant exiting the porous wall on the hot gas side forms a protective cooling film which reduces the heat load on the structure. The high cooling efficiency compared to conventional film cooling or regenerative cooling has been known since the 1950s.[6] However, the lack of suitable permeable materials limited the use of transpiration cooling to thermally relatively low loaded structures like the sintered stainless steel injector head face plate of the Space Shuttle Main Engine or the RL-10 upper stage engine.[27]

The development of porous ceramic matrix composite (CMC) materials like carbon fiber reinforced carbon (C/C) or the porous OCTRA material based on C/C-SiC ceramics[5] has lead to novel approaches for combustion chamber design which were intensively investigated at the DLR Institute for Stuctures and Design.[18] Furthermore, with recent progress in the additive manufacturing of structures with defined porosities,[14] the implementation of transpiration cooling in a additively manufactured rocket combustion chamber could be envisioned. Additive manufacturing is considered a key technology in the manufacturing of novel rocket engine combustion chambers. Numerical studies of transpiration cooled rocket engines using liquid oxygen (LOx) and liquid hydrogen (LH$_2$) as propellants were performed e.g. by Kacynski and Hoffman.[11] This study uses the NASA-developed Navier-Stokes solver Tethys. For simplification, a perfectly combusted fuel-rich hydrogen/oyxgen mixture was used for modeling the hot gas flow field. Furthermore, a thermal equilibrium between the coolant fluid and solid was assumed, meaning that the fluid has the same temperature as the solid wall material during the through-flow of the porous wall. A detailed study of transpiration cooling in a CH$_4$/LOx rocket engine was conducted by Bucchi et al.[1] In this study, the main driving parameters for the transpiration cooling performance were identified as the thermal conductivity, coolant injection temperature and the porosity, which implicitly influences the permeability and volumetric heat transfer. As transpiration and regenerative cooling have their specific advantages, it is likely that a optimal combustion chamber cooling system design will be a combination of different cooling methods for different regions adapted to local thermal loads. A possible design approach which was investigated using computational fluid dynamics is presented in the following, combining regenerative cooling in the thermally low loaded areas, as well as transpiration cooling in the thermally high loaded nozzle throat area.

The aim of this work is to present the development of numerical tools for the development and analysis of transpiration cooled rocket combustion chambers in the scope of multiple master theses[2,19,22] in the German Collaborative Research Center SFB TRR40. The simulation framework is applied to the TCD2 virtual Thrust Chamber Demonstrator developed by ArianeGroup in the framework of the TRR40, which was created to give a realistic test case for the results of fundamental research on rocket engines.

The TCD2 is a virtual main stage gas generator cycle rocket engine using LH$_2$ and LOx as propellants. The thrust chamber design is comparable to the European Vulcain 1 and Vulcain 2 rocket engine of the Ariane 5 launch vehicle. The key characteristics of the TCD2 virtual thrust chamber are given in Table 1. Aiming on lower rocket engine mass and cost, the main research goal of the TCD2 is to reduce the cooling channel pressure loss, putting less demands on the turbopump pressure gain.[8] One investigation approach is the implementation of transpiration cooling instead of conventional regenerative cooling in thermally high loaded areas, as shown in this paper.

2. Numerical Model

In the following, a brief description of the simulation framework is given. The simulations were performed using the commercial computational fluid dynamics solver ANSYS CFX 20.2, which models the Reynolds-averaged Navier-

Table 1: Description of the TCD2 virtual thrust chamber demonstrator[3]

	Symbol	Unit	
Propellant Combination		-	LH$_2$/LOx
Fuel/Oxidizer ratio	*ROF*	-	6
Chamber Pressure	p_c	bar	100
Total mass flow rate	$\dot{m}_{tot}$	kg/s	238.67
Thrust	*F*	kN	1000

Stokes equations using a finite volume approach.

The numerical framework is based on previous works by Munk et. al.[15] A coupling approach was proposed, in which the problem of a porous structure exposed to a hot gas flow was separated into a fluid domain representing the hot gas flow and a porous subdomain. In this "Two-Domain"-approach, both domains are solved independently. The results of the initial simulation are used as a boundary condition for further iterations, until the difference at the interface of both domains falls under the convergence threshold. CFX's internal feature for porous media flows uses a basic Representative Element Volume (REV) method that treats the fluid in the porous wall like one in a fluid domain and couples it with the solid using volumetric flow terms only. This means that in the momentum equations the fluid-porous interface is treated as a fluid-fluid interface, effectively creating a slip-wall condition. For the grid resolutions used in this work, a no-slip condition is required at the interface, using CFX's internal model leads to errors as the boundary layer is modeled incorrectly.[15] The described numerical setup was validated with the results of transpiration cooling experiments perfomed in the scope of TRR40.[15,20] In these fundamental research experiments, carbon fiber reinforced carbon (C/C) flat samples were perfused by air and exposed to a fully turbulent subsonic hot air flow with a temperature of T_{HG} = 373 K.

The described approach was modified for the investigation on the potential of transpiration cooling on rocket engine combustion chambers. The above mentioned approach does not include simulation of the coolant side of the cooling system. To be able to model the whole cooling system, a backside coolant reservoir was added. Due to numerical stability issues, two different coupling approaches approach were developed. The first approach was the addition of a backside coolant reservoir to the Two-Domain model, as a third domain. The Volumetric approach was developed as a further approach, with a monolithic fluid/solid domain and a porous domain. A detailed description of the respective approaches is given in subsection 2.1.

The investigated segment of the TCD2 virtual thrust chamber demonstrator is displayed in Figure 2, spanning from the injector faceplate to the nozzle extension interface. Due to the rotational symmetry of the investigated problem, only a 1/312 slice of the combustion chamber is simulated, which represents a full cooling channel in the regeneratively cooled part of the thrust chamber. For simplification, the cooling channel is not fully resolved, but is modeled only as a quasi-2D channel. Based on experimental studies on porous CMC combustion chamber liners,[9] the wall thickness of the porous segment was set to 10 mm. For the regeneratively cooled section, the wall was modeled assuming to be made of oxygen free high conductive copper (OFHC) with a 1 mm thickness.
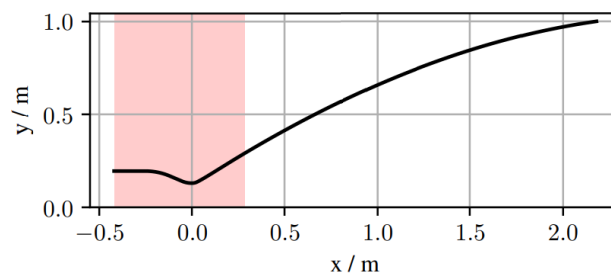
Figure 2: Geometry of the TCD2 virtual thrust chamber - Investigated segment marked in red

For the adoption of the framework on combustion chamber applications, special emphasis has to be laid on the modeling of the hot gas flow. In the presented study, two different approaches are being presented in Subsection 2.1 with a non-reactive hot gas model on the one hand as well as the modeling of a reactive hot gas flow.

Adoptions of the Two-Domain approach framework on thrust chamber applications, without a fully resolved coolant reservoir, can be found in Munk et al.[16,17]

2.1 Coupling Approaches

In the following, the Three-Domain and Volumetric coupling approaches are described in detail. Both approaches were implemented with a Python script externally coupling the respective domains set up in CFX.

2.1.1 Three-Domain Coupling

For the Three-Domain Coupling approach, the coolant reservoir was added to the existing framework as a second fluid domain, sharing an interface with the backside of the porous domain.[22] The porous-reservoir coupling was added in a similar manner as the hot gas-porous coupling from the Two-Domain approach. Figure 3 shows the numerical framework for the Three-Domain coupling approach. Initially, both the hot gas domain and the reservoir domain are
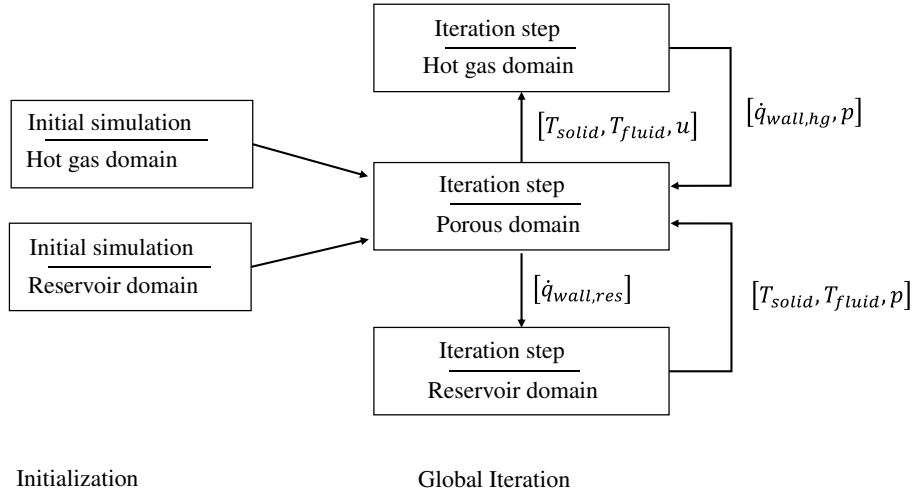
Figure 3: Numerical Framework for the Three Domain approach

solved with initial values on the interface to the porous wall, creating the thermal and pressure boundary conditions for the porous domain. Afterwards, the porous domain is solved, with the results at the hot gas- and reservoir interface updating the porous domain boundary conditions for the next global iteration step. This global iteration loop proceeds until the differences at the domain interfaces have fallen below the global convergence threshold. The respective boundary conditions for each domain are depicted in Figure 4.

For the hot gas-porous interface $\Gamma_{IF,HG-P}$, in accordance with the Two-Domain approach from Munk et. al.,[15] the wall heat flux determined from the hot gas simulation is set as a boundary condition, as well as the pressure distribution over the combustion chamber wall. In the hot gas domain, the density and velocity distribution ρ and $\vec{u}$ taken from the porous domain simulation are set for the mass source at the interface, as well as the interface solid and fluid temperatures. Similarly, hot gas-solid interfaces $\Gamma_{IF,HG-S}$ are coupled by exchanging the wall heat fluxes and temperatures, respectively.

At the reservoir-porous interface $\Gamma_{IF,R-P}$, the boundary conditions for the porous domain are the pressure at the reservoir wall p_s as well as the reservoir wall temperature distribution T_w. T_w can be split into a solid and a fluid fraction T_s and T_f following

$$T_w = \epsilon T_f + (1 - \epsilon) T_s \tag{1}$$

with ϵ being the porosity of the material. For the reservoir domain, the resulting coolant mass flow rate $\dot{m}$ from the porous domain is set as a mass sink boundary condition, as well as the heat flux at the porous inlet.

In order to achieve numerical stability, the boundary conditions for the heat transfer have to be under-relaxed using the formulation for the iteration step n

$$x_{relax}^n = (1 - r)x_{relax}^{n-1} + r \cdot x^n \tag{2}$$
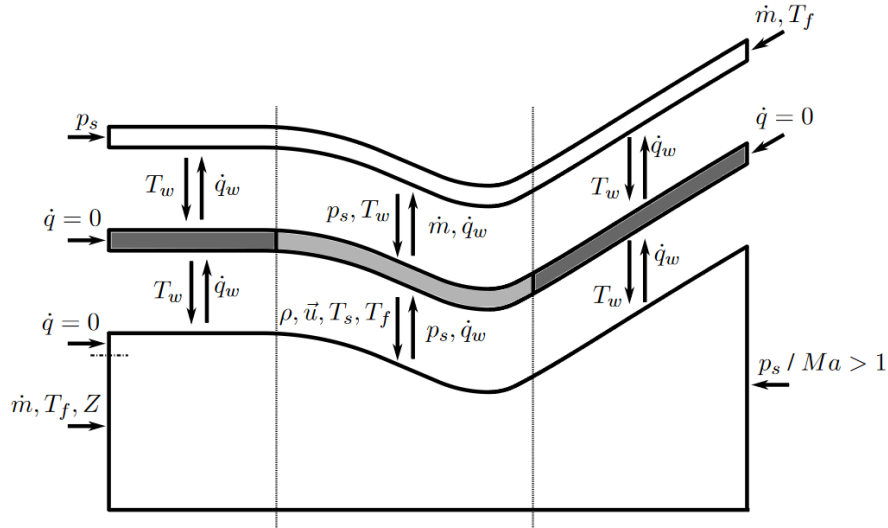
Figure 4: Boundary and interface conditions for the Three Domain coupling approach[19]

with x demarking the respective boundary conditions, r demarks the relaxation factor with $0 < r < 1$. For receiving a numerically stable solution, the relaxation factors for the hot gas side have to be fine-tuned for each specific case, with low relaxation factors of $r = 0.1 - 0.2$. However, persisting stability problems on the interface between the porous and hot gas domain and in the coolant domain lead to the development of a numerically more stable coupling approach.

2.1.2 Volumetric coupling approach

Due to the numerical stability issues described in Section 2.1.1, the coupling framework was modified to the Volumetric coupling approach.[19]

The whole setup is reduced to two domains, a fluid/solid and a porous domain, respectively. The framework is schematically described in Figure 5. The fluid/solid domain comprises of the hot gas domain from the Three-Domain approach, the regeneratively cooled solid walls in the cylindrical and divergent nozzle section as well as the cooling channel and transpiration coolant reservoir. In contrast to a straightforward monolithic approach, the porous section is modeled as a solid wall, for simulating the fluid-solid interaction with the coolant and hot gas, respectively. The transpiration cooling is modeled with the respective source and sink terms at the interface to the hot gas and reservoir. The internal heat transfer in the porous material is modeled with a volumetric heat sink term. The porous domain has the same setup as in the Three-Domain approach.
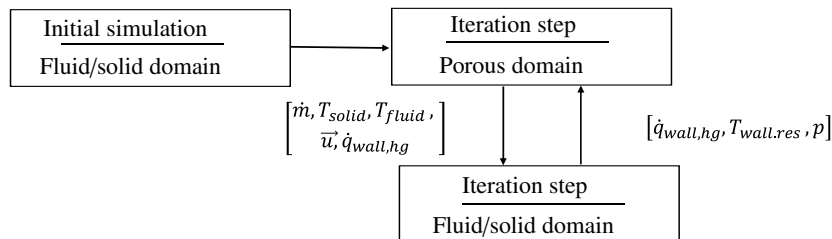
Figure 5: Numerical Framework for the Volumetric approach

The boundary and interface conditions for the Volumetric coupling approach applied to the investigated problem are shown in Figure 6. The framework was validated using results of Schweikert et. al.,[24] showing good agreement with the respective velocity and temperature profiles measured over a flat porous C/C sample exposed to a hot gas flow, as well as the sample wall temperature on the hot gas side.[19] The validation simulations gave similar results as the ones performed with a baseline Two-Domain coupling approach. However, for the reservoir side, significantly lower wall temperature were determined from the simulations compared to experimental data. Hence, lower temperatures are to be expected in the coolant reservoir. However, for this specific problem, no experimental data for the backside heat transfer exists for validation.
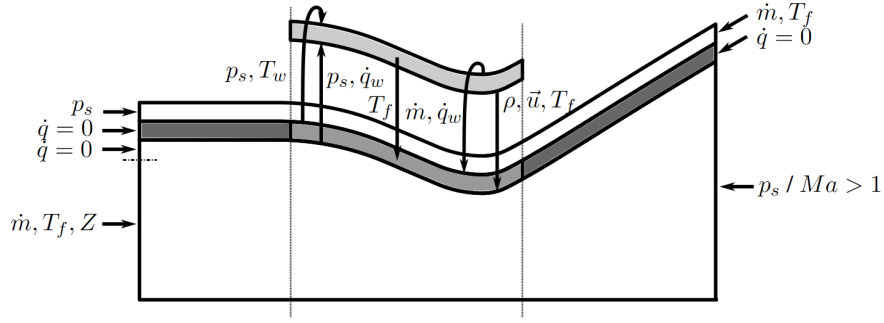
Figure 6: Boundary and interface conditions for the Volumetric approach[19]

2.1.3 Convergence criteria

Global convergence is achieved when the mean differences of $\dot{q}_w$, T_s and T_f for two successive iteration steps falls under the convergence threshold of 10^{-4}

$$\overline{\frac{|\dot{q}_{w,n}(\vec{x}) - \dot{q}_{w,n-1}(\vec{x})|}{|\dot{q}_{w,n}(\vec{x})|}} < 10^{-4} \qquad (3)$$

and

$$\overline{\frac{|T_{s,n}(\vec{x}) - T_{s,n-1}(\vec{x})|}{T_{s,n}(\vec{x})}} < 10^{-4} \qquad (4)$$

$$\overline{\frac{|T_{f,n}(\vec{x}) - T_{f,n-1}(\vec{x})|}{T_{f,n}(\vec{x})}} < 10^{-4} \qquad (5)$$

2.2 Porous Domain

The porous combustion chamber liner is modeled as a porous domain in CFX, using the implemented superficial loss formulation. In this formulation porous wall is modeled as a fluid domain, with loss terms in the momentum conservation equation based on Darcys law with the Forchheimer modification considering turbulent effects[12]

$$0 = \frac{dp}{dx} - \frac{\mu}{K_D} u_D - \frac{\rho}{K_F} u_D^2. \qquad (6)$$

K_D and K_F are the Darcy and Forchheimer coefficients, modeling the pressure loss for a specific porous medium with a superficial Darcy velocity u_D instead of the real pore velocity. A directional loss model can be implemented as the assumed materials for a transpiration cooled engine may have an anisotropic permeability, like e.g. ceramic matrix composites. Due to the small pore size of the porous materials, laminar flow was assumed for the through-flow of the coolant. On the inlet boundary on the reservoir side, the given boundary conditions from the reservoir simulation are the coolant temperature and the static pressure in the reservoir taken. Furthermore, the wall heat flux on the porous wall in the reservoir simulation is given as a boundary source on the cold gas side. On the interfaces to the solid walls in the cylindrical and divergent section, the walls are set to a free slip boundary condition. This is due to modeling the porous domain as a fluid domain. The free slip condition prevents here the non-physical formation of a boundary layer at the interface, as the fluid is modeled as a continuous volume. The heat transfer between the fluid and the solid part is modeled via the volumetric heat transfer coefficient h_v. Based on a conservative estimation for C/C by Schweikert,[23] $h_v = 10^6$ W m^{-1} K^{-1} was set for all investigated cases. For the fluid in the porous section, the hydrogen coolant has to be modeled taking real-gas behavior into account, as effects like the Joule-Thompson-effect are expected due to the expansion in the porous wall.[2] The coolant properties were defined by Real Gas Property (RGP) files which contain the fluid properties depending on temperature and pressure, as well as the full phase diagram. The hydrogen coolant is assumed to be in the parahydrogen isomeric state, as this is the state used typically in rocket engines due to the cryogenic storage temperatures.[4]

2.3 Hot gas flow modeling

In the following subsections, two different approaches for modeling a representative hot gas flow for the given TCD2 combustion chamber are being presented. On one hand, a non-reactive model well as a reactive model modeling the combustion processes in the combustion chamber. The hotgas flow simulations without transpiration cooling using the ArianeGroup in-house fluid dynamics solver Rocflam3[7] were used as a reference for the implementation into the existing CFX setup from DLR.

2.3.1 Non-reactive model

The first approach to model the hot gas flow in the combustion chamber is the usage of a non-reacting replacement gas.[22] As chemical reactions are to be neglected, the investigated section is reduced to the convergent-divergent thrust chamber section as shown in Figure 7. Based on an energy balance analysis of the reference combustion simulation, the flow in this segment is assumed to be chemically frozen. Furthermore for the applicability of transpiration cooling,
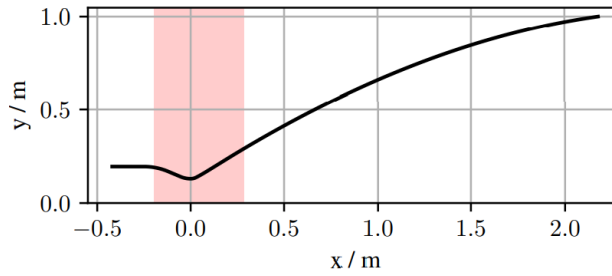
Figure 7: Shortened geometry for non-reactive flow modeling

this section is also the most interesting, as the highest thermal loads are around the nozzle throat. The replacement gas modeling the hot gas flow is assumed to be a single-species ideal gas so the thermodynamic properties viscosity μ, thermal conductivity k and specific heat capacity c_p can be described by a polynomial function

$$\Psi(T) = a_0 + a_1 \cdot T + a_2 \cdot T^2 + a_3 \cdot T^3. \tag{7}$$

The frozen flow assumption is based on a chemical equilibrium analysis using NASA CEA, assuming a 1D flow and isentropic nozzle flow. The mole and mass fractions are given in Table 2

Table 2: Mole and mass fraction of each apparent species at the inlet, nozzle throat and outlet of the investigated segment

Species i	M_i [g/mol]	$w_{i,inlet}$ [-]	$w_{i,throat}$ [-]	$w_{i,outlet}$ [-]
H_2O	18.0153	0.89995	0.91620	0.96273
H_2	2.01588	0.03709	0.03639	0.03501
OH	17.0073	0.05093	0.03904	0.00200
H	1.00794	0.00224	0.00184	0.00021
O_2	31.9988	0.00654	0.00444	0.00003
O	15.9994	0.00314	0.00203	0.00001
HO_2	33.0067	0.00007	0.00004	0.00000
H_2O_2	34.0147	0.00003	0.00002	0.00000

The coefficients of the polynomic equations are determined by fitting the flow field to the baseline Rocflam3 combustion simulations. The boundary conditions at the hot gas inlet are the total temperature and total pressure profiles extracted from the Rocflam3 simulations given at the specific inlet cross section of the shortened geometry. As for the porous domain, the hydrogen injected at the porous-hot gas interface is modeled as a real gas using an RGP table. Due to the foreign gas injection in the transpiration cooling, the main stream flow is modeled as a multi-component flow in CFX. Here, both components are ideally mixed on a molecular level, sharing the same pressure, temperature, velocity and turbulence fields. Turbulence is modeled using Menter's Shear Stress Transport Model, which blends the classical k-ω-model with a Wilcox k-ϵ-model in the free stream flow, leading to less freestream sensitivity.[13] The model was chosen due to its simplicity and its good agreement with experimental data in model combustion chambers found in the literature.[10,28] As an important tuning parameter for the wall heat flux, the turbulent Prandtl number was

NUMERICAL INVESTIGATION OF A TRANSPIRATION COOLED COMBUSTION CHAMBER

Table 3: Coefficients for thermophysical properties of the non reacting hot gas for Equation 7

Property	Symbol	a_0 [*]	a_1 [*/K]	a_2 [*/K^2]	a_3 [*/K^3]
Specific heat capacity	$c_p(T)$	$2.84425798 \cdot 10^3$	1.74574666	$-9.86386284 \cdot 10^{-4}$	$2.61495992 \cdot 10^{-7}$
Viscosity	$\mu(T)$	$-1.02333176 \cdot 10^{-7}$	$3.80954392 \cdot 10^{-8}$	$-3.16745201 \cdot 10^{-12}$	-
Thermal Conductivity	$k(T)$	$-1.385533488 \cdot 10^{-2}$	$2.58227599 \cdot 10^{-4}$	$-3.66447091 \cdot 10^{-8}$	$1.15117380 \cdot 10^{-11}$

* denotes the SI unit of the respective thermophysical property

set to $Pr_t = 1$ which resulted in the best fit for the wall heat flux. Figure 8 shows the resulting wall heat flux in a fully regenerative cooled configuration. A good agreement of the non-reactive model to the baseline Rocflam3 simulation is achieved in the convergent section and the nozzle throat ($x \leq 0m$). In the divergent section, the non-reactive model overestimates the heat flux slightly.
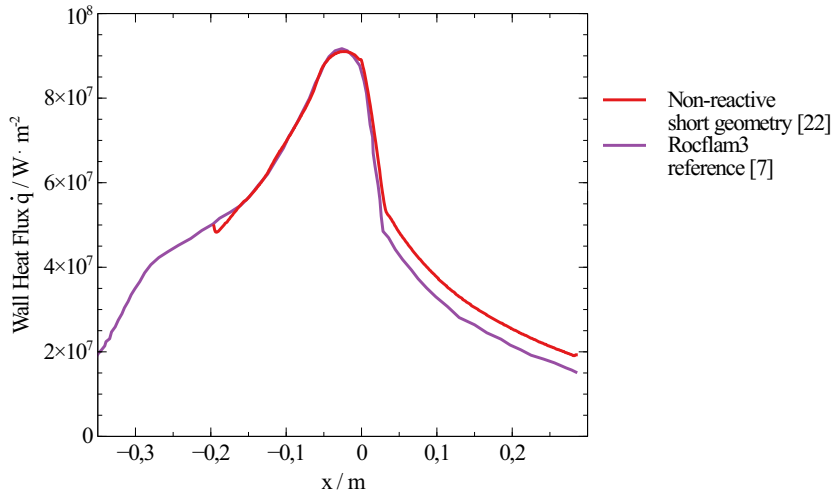
Figure 8: Comparision of the wall heat flux to the Rocflam3 results

2.3.2 Reactive flow model

Additionally to the non-reactive model, a hot gas model including combustion processes was set up in CFX. The combustion model used for the hot gas flow is the laminar flamelet model which is described by Peters.[21] This model is based on the assumption that the combustion process is confined to small sheets, taking the form of a representative laminar diffusion flame. This concept is advantageous due to its low computing time, as the combustion chemistry is included into the fluid dynamics simulation via pre-calculated lookup tables. Flamelet models require a probability density function (PDF) which couples the mixture fraction Z to the mass fractions of the physical species in the mixture. For CFX, the PDF is assumed to be a β-distribution, requiring both the mixture fraction Z and the mixture fraction variance Z'' for parametrization, which are both treated as conserved variables. It is assumed that the thin layers in which the flamelets are correspond to the smallest scales of turbulent motion. Thus, the flamelet assumption can be made if the expected flame thickness δ is smaller than a Kolmogorov eddy. It is assumed, that everywhere else, flame stretching and low mixture rates do not allow for a sustained flame.

To implement the flamelet model in CFX, the chemistry of the representative flame has to be tabulated. This was achieved using the RIF (Representative Interacting Flamelet) tool implemented in CFX 17.4, which calculates the mass fraction of the reactive components as a function of the mixture fraction and its variance, as well as the scalar dissipation rate and integrates it over the PDF. For the flamelet table generation, all fluids are assumed to be an ideal gas at an injection temperature of 100 K and an injection pressure of 100 bar. The fuel and oxidizer injection are modeled, with a single mesh cell resolving the injector post tip. For the investigated combustion chamber circular segment, 11 injector elements are modeled, with injection temperatures of 95 K for oxygen and 110 K for hydrogen. In accordance to the non-reacting model, turbulence is modeled using a SST model.

As well as for the non-reacting model, the combustion simulation was validated using Rocflam3 simulations of the full combustion chamber. Figure 9 shows the temperature distribution of the CFX simulation with the reactive flow model to the reference Rocflam3 simulation. The stoichiometric isosurface is depicted in black as a representative parameter
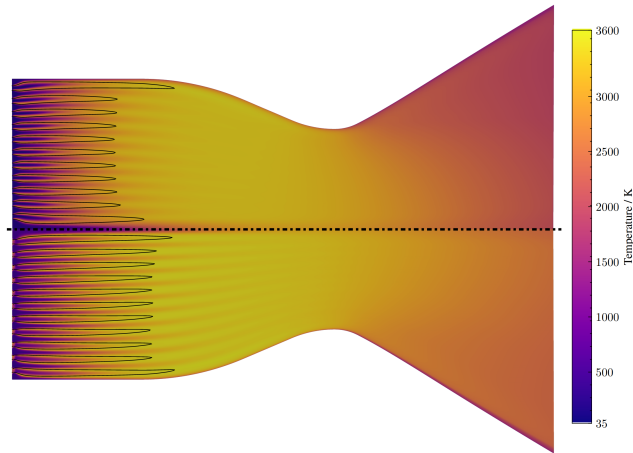
Figure 9: Temperature contour plot for CFX with combustion processes (upper) vs Rocflam3 (lower)[19]

for the position of the flame front. The difference in flame length could be attributed to the usage of the SST turbulence model, with the wall-nearest flame being affected of the k-ω turbulence model and the inner flames are modeled by a k-ϵ turbulence model. Furthermore, for the flame length, a strong dependency on the turbulent Prandtl Pr_t and Schmidt Sc_t numbers could be found. As a constraint of the flamelet model, a unity Lewis number Le is required. In order to obtain the best fit to the baseline calculations, Pr_t and Sc_t were set to 0.6. Furthermore, the different modeling approaches between Rocflam3 and CFX can attribute to differences in the hot gas flow field. For the flamelet model, strain rate dependent flame extinction is resolved, leading to a chemical frozen flow, locally. In contrast, the chemical equilibrium model implemented in Rocflam3 assumes the chemical kinetics to be significantly faster than the flow timescale. The flamelet model is limited to only a particular pressure, in this case the combustion chamber pressure of 100 bar. However, due to the significant pressure drop in the nozzle flow, the effect on the chemical reactions due to the pressure drop is not accounted for. This effects can be seen in the chemical composition of the hot gas flow

(a) OH mass fraction
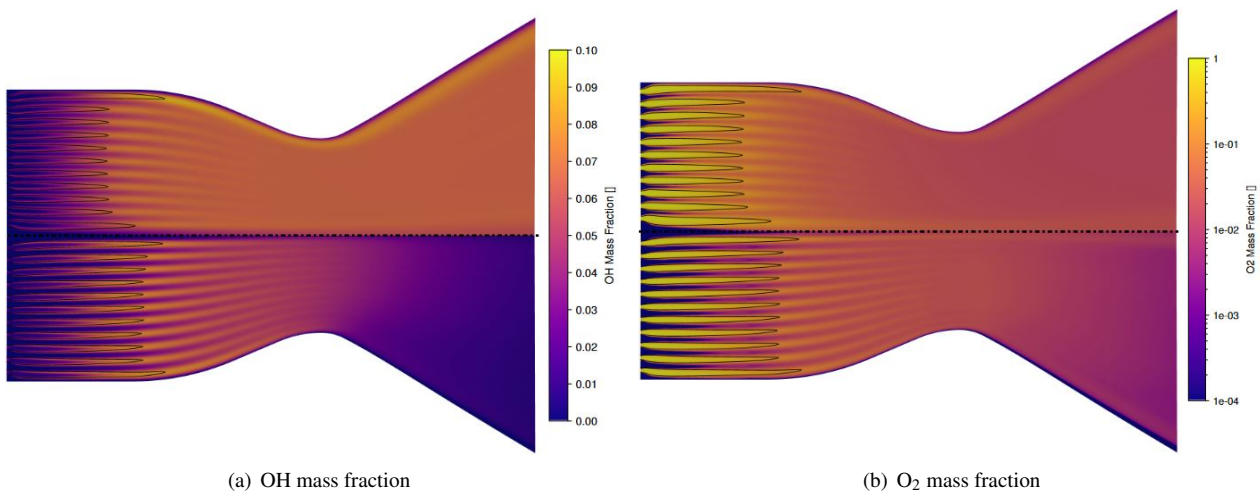
(b) O$_2$ mass fraction

Figure 10: Comparison of mass fractions between CFX with combustion processes(upper) and Rocflam3 (lower)[19]

field, as shown in Figure 10. Subfigure 10(a) shows the local OH mass fraction for both the adiabatic flamelet and the Rocflam3 simulations. This species appears only as an intermediate species during the hydrogen/oxygen combustion process. When using an chemical equilibrium model, the OH species is almost completely consumed, being mainly apparent in the flame front. For the adiabatic flamelet model, a significant amount of OH radicals remains high in the wake of the flame in the nozzle flow. Furthermore, the completeness of the combustion is can be interpreted via the mass fraction of molecular oxygen. Due to the fuel-rich oxidizer/fuel ratio of 6 for the investigated thrust chamber, the amount of molecular oxygen should be negligibly small. In Subfigure 10(b) the oxygen mass fraction distribution for both combustion models is being displayed . Here, it can clearly be seen, that significantly more oxygen is apparent in the nozzle section of the combustion chamber for the Flamelet model compared to the Rocflam3 calculations, meaning

that the combustion process is not modeled complete and freezes too quickly in contrast to the expected result.

3. Comparison of hot gas models

In Figure 11, the wall heat flux distribution on the combustion chamber with a fixed wall temperature is shown using the described hot gas models as well as the Rocflam3 results from Eiringhaus et al.[7] The non-reactive model is applied to the full combustion chamber, giving the total mass flow and a temperature of T = 3500 K as boundary conditions at the combustion chamber injector face plate.
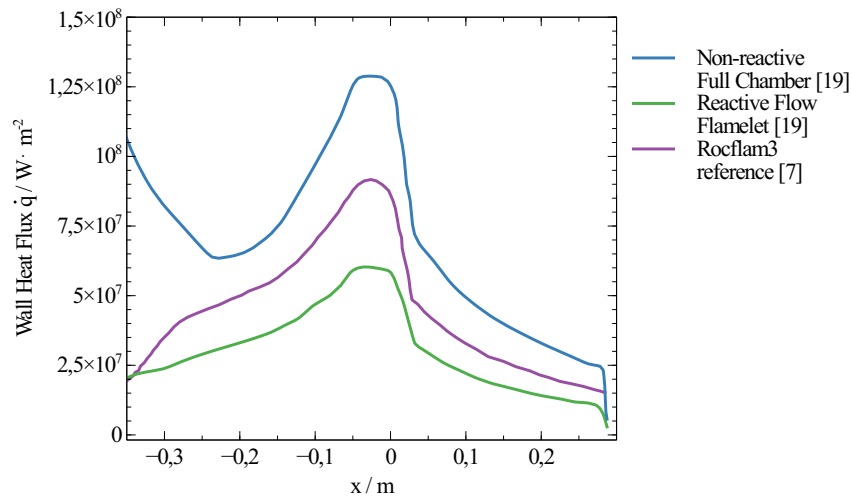
Figure 11: Comparison of the wall heat flux for different hot gas models

When applied to the full chamber, the non-reactive model shows a significant overestimation of the heat flux, with the maximum heat flux near the nozzle throat being 40% higher than the baseline calculation. This can be attributed to the neglection of the change in gas composition as well as the the turbulent Prandtl number, which was used as a tuning parameter for fitting the heat flux to the Rocflam3 calculation in the shortened geometry. This shows, that for a good agreement for such a model, as shown in Figure 8, the inlet boundary conditions have to be known exactly. For applying a non-reactive model to a full chamber geometry the gas properties as well as the turbulent Prandtl number have to be adapted in order to match the heat transfer characteristics determined from the reactive flow simulation. For the reactive flow model, the heat fluxes are significantly lower. This can be attributed to the different combustion modeling approaches used for Rocflam3 and CFX, as already described in chapter 2.3.2. Due to the incomplete combustion and therefore significantly lower temperatures of the hot gas results in lower wall heat fluxes. However, the resulting wall heat flux curve shows the distinctive distribution. In general, the usage of combustion modeling for the hot gas flow allows a greater flexibility for the specific use cases, requiring only the injection conditions.
In the following study the volumetric coupling approach is used due to its improved numerical stability. The hot gas is modeled with the reactive flow model. However, with transpiration cooling, it could be found that the reactive flow model didn't fully converge globally, with residuals of $O(10^{-2})$.

4. Parametric study

The choice of a suitable material of the combustion chamber is crucial for the performance of the transpiration cooling. As shown by Bucchi et. al.,[1] the main material properties driving the performance of transpiration cooling are the thermal conductivity of the bulk material k and the porosity ϵ. In the following study, the influence of the porosity is only indirectly investigated, as it is assumed to directly influence the transpired mass flow rate due to the change of permeability at fixed pressure boundary conditions. As the pressure in both the plenum and inside the combustion chamber are given through the investigated use case, the permeability of the porous wall is the main driving factor for the amount of coolant used in the transpiration cooling. For simplification, the permeability was assumed to be isotropic. For the thermal conductivity and porosity, the properties were set to match the values of the carbon fiber reinforced carbon (C/C) material as given in Table 4. The Darcy and Forchheimer coefficients were varied between $K_D = 10^{-12}\text{-}10^{-14}$ m^2 and $K_F = 10^{-8}\text{-}10^{-10}$ m as given in Table 5.

Table 4: Properties of Carbon Fiber Reinforced Carbon (C/C)

Property	Symbol	Unit	Value
Thermal Conductivity perpendicular to fiber orientation	$k_\perp$	W·(m· K)$^{-1}$	2.22
Thermal Conductivity parallel to fiber orientation	$k_\parallel$	W·(m· K)$^{-1}$	16.41
Porosity	ϵ	-	0.111

Table 5: Test cases variation of permeability

	Symbol	Unit	Case 1.1	Case 1.2	Case 1.3	Case 1.4	Case 1.5
Darcy coefficient	K_D	m^2	10^{-14}	$5\cdot 10^{-14}$	10^{-13}	$5\cdot 10^{-13}$	10^{-12}
Forchheimer coefficient	K_F	m	10^{-10}	$5\cdot 10^{-10}$	10^{-9}	$5\cdot 10^{-9}$	10^{-8}

The resulting wall temperatures and wall heat fluxes are given in Figure 12. It can be seen, that the cooling effect rises significantly with higher permeabilities, due to the rising amount of coolant which perfuses the porous wall. For Case 1.5, the heat flux on the porous wall could be significantly reduced from an average wall heat flux of 6.06 MW/m^2 for Case 1.1 to 0.493 MW/m^2 in Case 1.5. However, for the lowest permeability, peak wall temperatures of over 2400 K could be determined, which are too high for the materials which would be potentially used for a transpiration cooled engine. A permeability similar to Case 1.2 seems to be the most viable, with the peak temperature of 1400 K being significantly below the maximum temperature of 2000 K for the given C/C material. Another phenomenon is the formation of a coolant film, which can be seen through the strong temperature reduction in the divergent part of the nozzle. Here, most interestingly for the cases 1.4 and 1.5, a significantly low wall temperatures could be determined in the wake of the porous segment, indicating a film cooling effect even until the end of the investigated thrust chamber segment. The resulting coolant mass flow rates to the investigated cases are given in Table 6. The transpired mass flow rate can be expressed in a non-dimensional form, the blowing ratio

$$F = \frac{\dot{m}_c/A_c}{\dot{m}_{hg}/A_{hg}} \tag{8}$$

where $\dot{m}_c/A_c$ denotes the coolant mass flux at the hot gas/porous wall interface and $\dot{m}_{hg}/A_{hg}$ denotes the mass flux of the hot gas evaluated at the cylindrical section of the combustion chamber, with $\dot{m}_{hg}/A_{hg} = 7727.84$ kg m^{-2}s^{-1}.
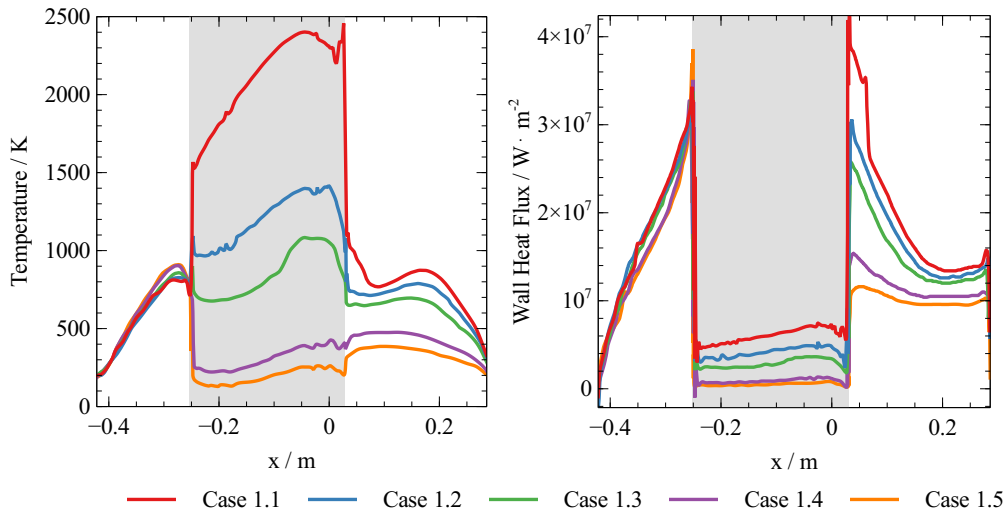
Figure 12: Temperatures (left) and Wall heat fluxes (right) with different permeabilites[19]

NUMERICAL INVESTIGATION OF A TRANSPIRATION COOLED COMBUSTION CHAMBER

Table 6: Resulting coolant mass flow rates

	Symbol	Unit	**Case 1.1**	**Case 1.2**	**Case 1.3**	**Case 1.4**	**Case 1.5**
Coolant mass flow rate	$\dot{m}_c$	$kg \cdot s^{-1}$	0.89	3.87	6.61	18.94	27.38
Blowing ratio	F	%	0.039	0.17	0.29	0.83	1.2
Fraction of total propellant mass flow rate	$\dot{m}_c/\dot{m}_{Propellant}$	%	0.39	1.68	2.87	8.21	11.87

5. Conclusion and Outlook

A numerical framework for the thermal analysis of transpiration cooled rocket combustion chambers based on the commercial CFD solver ANSYS CFX was developed. The framework was demonstrated on the virtual thrust chamber demonstrator TCD2. The transpiration cooling was modeled using a fully coupled approach based on previous studies, extending the existing setup with the modeling of the backside flow in the coolant reservoir and the cooling channels. The coupling approach evolved from the addition of a backside plenum to the Volumetric approach, which proves numerically more stable for the usage of detailed parametric studies. For modeling the hot gas flow inside the combustion chamber, two different approaches were pursued. On one hand, a non-reactive approach was investigated, with an ideal replacement gas tuned to match the heat transfer characteristics of the reactive hot gas flow determined from combustion simulations. On the other hand, the hot gas was modeled as a reactive flow, implementing a flamelet combustion model. A comparison of the hot gas models showed that the non-reactive model can only be applied to the shortened geometry and hence overestimates the heat transfer significantly when applied to a full chamber. In contrast, the reactive flow simulation using the flamelet model had shown significantly lower heat fluxes than the reference calculation, due to the different combustion modeling approaches implemented in CFX and Rocflam3. Furthermore, the flamelet model didn't fully converge with transpiration cooling, hence for future studies, additional effort has to be put in the development of suitable reactive flow models. In the presented study, the potential of transpiration cooling in main stage LOx/LH$_2$ rocket engine could be demonstrated. Due to the usage of generic material properties in a parametric study, the influence of the permeability as a main driving factor for the cooling performance could be shown. The effectiveness of the transpiration cooling increases with higher permeabilities due to the increasing coolant mass flow rate. A significant heat flux reduction could be detected even in the wake of the porous segment, indicating a lasting cooling film formed by the transpired coolant. In this study, assuming a wall made of C/C as baseline, the desired permeability would be in the range of $K_D = 5 \cdot 10^{-14}$ m^2 and $K_F = 5 \cdot 10^{-10}$ m resulting in a total coolant mass flow rate of 3.87 kg/s for the given setup. The maximum wall temperature for the studied case is 1405 K, which is well below the allowed maximum temperature of CMC materials. High temperature ceramic matrix composites could have a high potential, but permeabilities have to be comparably low in order to fully utilize the potential to reduce coolant mass flow in the investigated test case. However, with the given framework, different classes of materials could be investigated for the usage in transpiration cooled rocket engines, such as e.g. additively manufactured porous metallic structures.

For future studies, the coupling approaches have to be validated under operation representative conditions, as the validation of the coupling is based only on simplified fundamental experiments of air cooled C/C-samples exposed to a hot air flow with moderate temperatures of 373 K. As this does not account for effects like foreign gas injection, real gas effects and combustion processes, further experiments on transpiration cooled sub-scale combustion chambers under realistic conditions have to be performed. Furthermore, the heat transfer at the reservoir-porous interface has to be further investigated to validate the coupling approach, as this is critical for determining the coolant temperature in the reservoir as an important parameter for the engine design.

6. Acknowledgments

References

[1] A. Bucchi, C. Bruno, and A. Congiunti. Transpiration Cooling Performance in LOX/Methane Liquid-Fuel Rocket Engines. *Journal of Spacecraft and Rockets*, 42(3):476–478, 2005.

[2] T. Cziep. Numerisch gekoppelte Simulation segmentierter Brennkammerkonfigurationen mit neuartigen Küh-lkonzepten. Master thesis, ITLR Vol. 105, University of Stuttgart, 2020.

[3] D. Eiringhaus and H. Riedmann and O. Knab. Definition and Evaluation of Advanced Rocket Thrust Chamber Demonstrator Concepts. In N.A. Adams et. al, editor, *Future Space-Transport-System Components under High Thermal and Mechanical Loads*, volume 146 of *Notes on Numerical Fluid Mechanics and Multidisciplinary Design*. Springer Nature, Cham, 2021.

[4] A. Dadieu, R Damm, and E. W. Schmidt. *Raktentreibstoffe*. Springer, Wien, New York, 1969.

[5] C. Dittert and M. Kütemeyer. OCTRA - Optimized Ceramic for Hypersonic Application with Transpiration . In M. Singh et al., editor, *Advances in High Temperature Ceramic Matrix Composites and Materials for Sustainable Development*, volume 263 of *Ceramic Transactions*. John Wiley & Sons, Hoboken, 2017.

[6] E.R.G. Eckert and J.N.B. Livingood. Comparison of effectiveness of convection-, transpiration-, and film-cooling methods with air as coolant. Technical Note 3010, National Advisory Commitee for Aeronautics, October 1953.

[7] D. Eiringhaus, H. Riedmann, and O. Knab. Virtual Liquid Propellant Thrust Chamber Demonstrators. In *Sonder-forschungsbereich/Transregio 40 Annual Report 2018*. Garching, 2018.

[8] D. Eiringhaus, H. Riedmann, O. Knab, and O. Haidn. Full-Scale Virtual Thrust Chamber Demonstrators as Numerical Testbeds within SFB-TRR 40. *2018 Joint Propulsion Conference*, 2018.

[9] H. Hald, M. Ortelt, I. Fischer, D. Greuel, and O. Haidn. Effusion cooled CMC rocket combustion chamber. *AIAA/CIRA 13th International Space Planes and Hypersonics Systems and Technologies Conference*, 2005.

[10] B. Ivancic, H. Riedmann, M. Frey, O. Knab, S. Karl, and K. Hannemann. Investigation of different modeling approaches for CFD simulation of high pressure rocket combustors. *5th European Conference for Aeronautics and Space Sciences*, 2013.

[11] K. J. Kacynski and J. D. Hoffman. The Prediction of Nozzle Performance and Heat Transfer in Hydrogen/Oxygen Rocket Engines with Transpiration Cooling, Film Cooling, and High Area Ratios. *30th Joint Propulsion Conference*, June 1994.

[12] Massoud Kaviany. *Principles of heat transfer in porous media*. Mechanical engineering series. Springer, New York, 2. ed., corr. 2. printing edition, 1999.

[13] F. R. Menter. Two-Equation Eddy-Viscosity Turbulence Models for Engineering Applications. *AIAA Journal*, 32(8):1598–312, August 1994.

[14] Z. Min, G. Huang, S. N. Parbat, L. Yang, and M. K. Chyu. Experimental investigation on additively manufactured transpiration and film cooling structures. *Journal of Turbomachinery*, 141(3), March 2019.

[15] D. Munk, M. Selzer, H. Böhrk, S. Schweikert, and G. Vio. Numerical modeling of transpiration-cooled turbulent channel flow with comparisons to experimental data. *Journal of Thermophysics and Heat Transfer*, 32(3):713–735, July 2018.

[16] D. Munk, M. Selzer, H Seiler, M. Ortelt, and G. Vio. Analysis of a transpiration cooled LOX/CH4 rocket thrust chamber. *International Journal of Heat and Mass Transfer*, 182:1–18, January 2022.

[17] D. Munk, M. Selzer, G. Steven, and G. Vio. Topology optimization applied to transpiration cooling. *AIAA Journal*, 57(1):297–312, January 2019.

[18] M. Ortelt, H. Hald, A. Herbertz, and I. Müller. Advanced Design Concepts for Ceramic Thrust Chamber Components of Rocket Engines. *5th European Conference for Aeronautics and Space Sciences*, 2013.

[19] P. Palmetshofer. Fully coupled numerical simulation of a transpiration cooled rocket thrust chamber with com-bustion modeling. Master thesis, ITLR Vol. 124, University of Stuttgart, 2021.

[20] J. Peichl, A. Schwab, M. Selzer, H. Böhrk, and J. von Wolfersdorf. Innovative Cooling for Rocket Combustion Chambers. In N.A. Adams et. al, editor, *Future Space-Transport-System Components under High Thermal and Mechanical Loads*, volume 146 of *Notes on Numerical Fluid Mechanics and Multidisciplinary Design*. Springer Nature, Cham, 2021.

NUMERICAL INVESTIGATION OF A TRANSPIRATION COOLED COMBUSTION CHAMBER

[21] N. Peters. *Turbulent Combustion*. Cambridge University Press, Cambridge, 2000.

[22] P. Pfannes. Numerisch gekoppelte Simulation einer Brennkammer mit neuartigen Kühlkonzepten. Master thesis, ITLR Vol. 75, University of Stuttgart, 2018.

[23] S. Schweikert. Ein Beitrag zur Beschreibung der Transpirationskühlung an keramischen Verbundwerkstoffen. PhD thesis, University of Stuttgart, 2019.

[24] S. Schweikert, J. von Wolfersdorf, M. Selzer, and H. Hald. Experimental Investigation on Velocity and Temperature Distributions of Turbulent Cross Flows over Transpiration Cooled C/C Wall Segments. *5th European Conference for Aeronautics and Space Sciences (EUCASS), Munich*, 2013.

[25] D. Suslov, R. Arnold, and O. Haidn. Investigation of two dimensional thermal loads in the region near the injector head of a high pressure subscale combustion chamber. *47th AIAA Aerospace Sciences Meeting including The New Horizons Forum and Aerospace Exposition*, 2009.

[26] G. P. Sutton and O. Biblartz. *Rocket Propulsion Elements*. John Wiley & Sons, Hoboken, NJ, 8 edition, 2010.

[27] L. R. Tully, A. Omar, J. N. Chung, B. F. Carroll, and P. K. Tucker. Fluid Flow and Heat Transfer in a Liquid Rocket Fuel Injector. *41th Joint Propulsion Conference*, July 2005.

[28] V. Zhukov. Modelling of Combustion and Heat Transfer in Rocket Combustion Chambers Using CFX. *ANSYS Conference & 33rd CADFEM Users Meeting 2015*, 2015.